Macromolecular
Rapid Communications
www.mrc-journal.de

Transformation from Nanofibers to Nanoribbons in Poly(3-hexylthiophene) Solution by Adding Alkylthiols

*Shuang Pan, Mingjing Zhu, Luze He, Hongdong Zhang, Feng Qiu, Zhiqun Lin, and Juan Peng**

An intriguing morphological transition from poly(3-hexylthiophene) (P3HT) 1D nanofibers to 2D nanoribbons enabled by the addition of a series of alkylthiols is reported. First, P3HT 1D nanofibers are formed due to strong anisotropic π–π stacking between planar rigid backbones. Upon the addition of alkylthiols, P3HT nanofibers are transformed into nanoribbons associated with the crystallographic transition from edge-on orientation to flat-on orientation. The content of alkylthiols has a great influence on the P3HT morphology in the solution. The mechanism of such a morphological transformation is discussed based on the interaction between alkylthiols and P3HT chains. This work offers an effective strategy to tailor the crystal morphology and dimension of P3HT, which not only improves the understanding of P3HT crystallization but also may enable such discovery into conjugated polymer-based optoelectronic devices.

1. Introduction

Conjugated polymers combine the optoelectronic properties of semiconductors and the good processability of polymers, which have been widely used in organic electronics such as organic photovoltaics (OPVs), light-emitting diodes (LEDs), thin-film transistors, etc.[1–3] Among various conjugated polymers, poly(3-hexylthiophene) (P3HT) is mostly studied due to its excellent charge carrier mobility and chemical stability.[4] For example, in bulk heterojunction (BHJ) solar cells, P3HT is a model compound as the electron donor and a fullerene derivative (e.g., [6,6]-phenyl-C_{61}-butyric acid methyl ester (PCBM)) is as the electron acceptor. The power conversion efficiency (PCE) of the model system (P3HT/PCBM) can be 3–5% with the performance highly related to the P3HT crystallinity and nanoscale morphology of the active layer composed of P3HT/PCBM.[5] Therefore, a lot of work has been done to control the crystalline structure of P3HT. Based on post-processing approaches such as thermal[6] or solvent annealing,[7,8] the crystallinity of P3HT can be greatly enhanced, which is favorable for the device performance. Besides, solution-processing approaches without thermal or solvent annealing have been effectively used. Since the crystallization of P3HT is sensitive to the solvents,[9] additives,[10] aging time, and temperature,[11] etc., its crystalline structure can be directly tailored in the solution, which is more attractive and efficient.

Among solution-processing approaches to tailor the P3HT crystallization, the addition of additives has attracted increasing attention. Since the first report on the additive to improve the device performance by Peet et al.,[10] some work have been done on this subject.[12–18] For example, the addition of alkylthiols to P3HT/PCBM was found to significantly improve the photoconductivity due to the enhanced structural order.[10] In another example, the mechanism about how alkylthiols affected the P3HT/PCBM morphology was investigated, in which *n*-dodecylthiol reduced the entanglement of P3HT chains and further promoted its coil-to-rod transformation.[12] It is worth noting that in most work, P3HT was dissolved in good solvents with flexible coil characteristic before the addition of additives. After the P3HT chains crystallize into nanofibrillar structures due to interchain π–π stacking, how the additives influence the already formed nanofibers remains unexplored.

In our previous report, a novel nanoribbon-shaped nanocomposites composed of P3HT nanoribbons and gold nanorods were crafted by a coassembly of thiol-terminated P3HT (P3HT-SH) nanofibers with dodecanethiol-coated gold nanorods.[19] The dissociated dodecanethiol (DDT) ligands from the gold nanorod surface was assumed to drive such intriguing nanofiber-to-nanoribbon transformation. However, the effects of the dodecanethiol on the P3HT crystallization including the interaction, kinetic process, transformation mechanism, etc. were not clear. Motivated by these thoughts, herein we go one step further, investigated the effect of a series of alkylthiols on the P3HT nanofibers in detail. The transformation kinetics and mechanism as well as the associated changes on their photophysical properties were scrutinized. The effect of the alkylthiol chain length on the P3HT morphology was explored. For comparison,

---

S. Pan, M. Zhu, L. He, Prof. H. Zhang, Prof. F. Qiu, Prof. J. Peng
State Key Laboratory of Molecular Engineering of Polymers
Department of Macromolecular Science
Fudan University
Shanghai 200433, China
E-mail: juanpeng@fudan.edu.cn

Prof. Z. Lin
School of Materials Science and Engineering
Georgia Institute of Technology
Atlanta, GA 30332, USA

The ORCID identification number(s) for the author(s) of this article can be found under https://doi.org/10.1002/marc.201800048.

DOI: 10.1002/marc.201800048

another four small molecules with similar alkyl length but different end functional groups were also used as additives. The significance of this work is to demonstrate an efficient strategy to tailor the crystal morphology and dimension of P3HT, which not only improves the fundamental understanding on P3HT crystallization but also may enable such discovery into conjugated polymer-based devices for use in organic field-effect transistors (OFETs), LEDs, solar cells, optical imaging, and sensors.

2. Experimental Section

2.1. Materials

P3HT ($M_n = 9500$, $M_w/M_n = 1.22$) was synthesized by Grignard metathesis polymerization (GRIM) with GPC data showed in Figure S1 in the Supporting Information.[20] 1-Heptanethiol, 1-dodecanethiol, 1-octadecanethiol, (we call them 7-thiol, 12-thiol, and 18-thiol in this paper, respectively) were purchased from Aladdin Industrial Corporation and used without further purification. *n*-Dodecane, dodecanoic acid, dodecyl amine, and oleylamine were purchased from Alfa Aesar. Methylene dichloride (CH_2Cl_2) and chloroform ($CHCl_3$) were used as received.

2.2. Sample Preparation

In a typical procedure, P3HT was dissolved in $CH_2Cl_2/CHCl_3$ mixed solution (volume ratio = 7:1, 0.5 mg mL^{-1}) and stirred at room temperature for 24 h to assure the formation of 1D nanofibers. Then, different amount of alkylthiols were added into the P3HT nanofiber solution and the final concentration of P3HT was kept at 0.25 mg mL^{-1}. For comparison, *n*-dodecane, dodecanoic acid, dodecyl amine, and oleylamine were also added into the P3HT nanofiber solution under the same condition. The mixed solutions were stirred overnight before characterization.

2.3. Characterization

Transmission electron microscopy (TEM) images and selected area electron diffraction (SAED) patterns were obtained on a Tecnai G^2 20, FEI electron microscope operated at 200 kV. TEM samples were prepared by drop-casting P3HT solutions onto carbon-coated copper grids, followed by evaporation of the solvent at ambient. Cryogenic TEM (cryo-TEM) was carried out using a Gatan cryo-holder operating at ≈−170 °C and FEI Tecnai G^2 20 Twin TEM at 200 kV. Atomic force microscopy (AFM) was carried out on Multimode 8 AFM Nanoscope IV in tapping mode. Thin films for AFM were prepared by spin-coating P3HT solutions on silicon wafers at 3000 r min^{-1} for 60 s. UV–vis spectroscopy was carried out on Perkin–Elmer Lambda 750 equipment using a quartz cuvette of 1 mm path length. Photoluminescence (PL) spectra were recorded on a FLS960 spectrophotometer (Edinburgh Instruments).

3. Results and Discussion

In a typical whisker method, P3HT can self-organize into semicrystalline nanofibers in anisole[21] or solvent-poor solvent mixture[22] through strong π–π stacking. In our case, P3HT formed 1D nanofibers in $CH_2Cl_2/CHCl_3$ mixed solution with high aspect ratio (**Figure 1**a). By AFM measurement, the nanofibers had the height, width, and length of ≈5 nm, 15 nm, and 2–3 µm, respectively (Figure 1b). The inset in Figure 1a was the corresponding SAED pattern of nanofibers, which showed only one diffraction ring assigned to crystallographic (020) plane with a *d*-spacing of 3.8 Å. It suggests that the electron beam goes along (100) direction, which proves that the P3HT chains adopt edge-on orientation with π–π stacks along the nanofiber long axis. According to the previous report that the thickness of a single molecular layer of P3HT in the side chain direction is ≈1.6 nm,[23] it indicates ≈3 layers of P3HT backbones perpendicular to the nanofiber long axis.

After adding a certain content of 12-thiol into the P3HT nanofiber solution, interestingly, an obvious morphological transformation from 1D nanofibers to 2D nanoribbons was observed, with the average nanoribbon height and width of ≈20 and 50–300 nm, respectively (Figure 1c,d). The corresponding SAED pattern showed four diffraction rings assigned to crystallographic (100), (200), (300), and (020) planes, respectively (inset in Figure 1c). It suggests that the electron beam goes along (001) direction, which proves that the P3HT chains adopt flat-on orientation in nanoribbons with the polymer backbones perpendicular to the film plane.[8,24] The *d*-spacing of the (100) plane was 16.74 Å and the π–π stacking distance was 3.84 Å, which could be attributed to form I crystal of P3HT with noninterdigitating side chains.[25] Since the solvent evaporation rates during the preparation of TEM and AFM samples were quite different, the consistent morphology measured by them indicated the dry sample represented the case in the solution. The cryo-TEM also showed a nanoribbon morphology, further demonstrating that the nanoribbons were formed in the solution instead of during the solvent evaporation process (Figure S2, Supporting Information). Notably, P3HT nanoribbons have been obtained in nanofiber anisole solution with the concentration above 0.2 mg mL^{-1} and aged at room temperature for a certain time, which differ largely from the present study by adding 12-thiol.[24] To compare these two kinds of nanoribbons, P3HT used in this study was also dissolved in anisole with the concentration of 0.5 mg mL^{-1} followed by aging. As we can see, 2D nanoribbons with the flat-on orientation were indeed formed in anisole characterized by both TEM and AFM (Figure S3, Supporting Information). The d_{100} and d_{020} of nanoribbons were 16.70 and 3.83 Å, respectively, which were slightly smaller than those of nanoribbons prepared with the addition of 12-thiol. By AFM measurement, the height of these nanoribbons was ≈16 nm, which was also ≈4 nm lower compared with the height of nanoribbons in Figure 1d. It is assumed that the 12-thiol intercalated into the P3HT molecules, which will be discussed in detail below.

It is interesting to note that the content of 12-thiol has great effects on the transformation of P3HT structure in the solution (**Figure 2**). When 12-thiol content was 1% by volume, only a few nanoribbons were observed coexisting with a number of nanofibers homogenously distributed in the film (Figure 2a). With the increased content of 12-thiol, more and more nanoribbons appeared accompanied by the decreasing of nanofibers obviously (Figure 2b–e). Further increasing the 12-thiol to 50%,

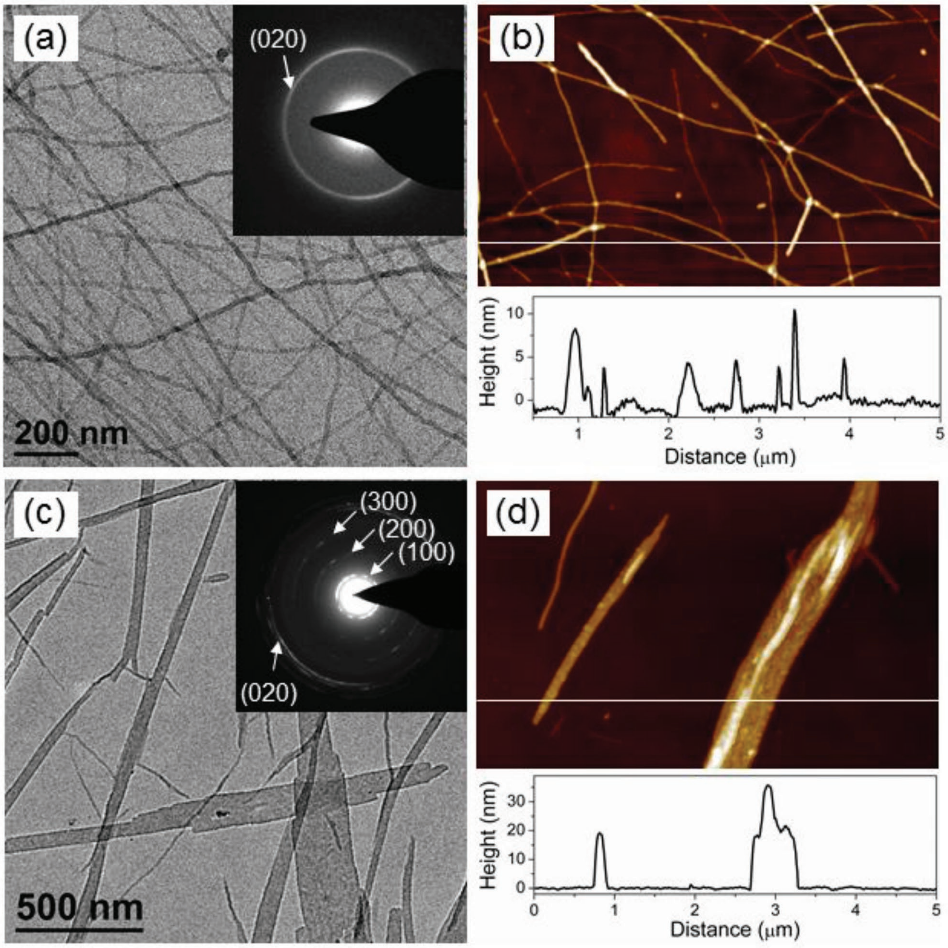

Figure 1. a) TEM image of P3HT nanofibers drop-cast from $CH_2Cl_2/CHCl_3$ solution. The inset is the corresponding SAED pattern. b) AFM image along with the line profile of P3HT nanofibers. c) TEM image of P3HT nanoribbons drop-cast from $CH_2Cl_2/CHCl_3$ solution with the addition of 12-thiol at 30% by volume. The inset is the corresponding SAED pattern. d) AFM image along with the line profile of P3HT nanoribbons.

only nanoribbons were observed (Figure 2f). It indicated that the transformation from P3HT nanofibers to nanoribbons was complete.

To explore the optical properties of P3HT during morphological transformation and find out the structure–property relationship, UV–vis absorption and PL spectra were performed. The initial P3HT nanofiber solution showed a main absorption peak at 454 nm and a shoulder peak at 596 nm, which are due to the intrachain π–π^* transition of P3HT main chain and the interchain π–π interaction, respectively (**Figure 3**a).[26] During the addition of 12-thiol, the intensity of the shoulder peak almost did not increase until the content of 50%, indicating the transformation of nanofibers to nanoribbons did not strengthen the π–π stacking of P3HT when the content of 12-thiol was below 50%. It was reasonable because the π–π stacking of P3HT chains had almost reached its equilibrium in the initial nanofiber solution.

From the corresponding PL spectra, the initial P3HT nanofiber solution exhibited two emissive peaks at 579 and 639 nm, which were assigned to the 0–0 and 0–1 intrachain singlet transitions, respectively (Figure 3b).[27] It is reported that P3HT chains in solution can exhibit photophysical behavior of J-aggregates (i.e., the 0–0 transition is enhanced relative to the 0–1 sideband) or H-aggregates (i.e., the 0–0 transition is less intense than the 0–1 sideband) depending on the dominance of intrachain or interchain exciton coupling, respectively.[28] In our system, the I_{0-0}/I_{0-1} remained less than 1 during the whole 12-thiol addition process, indicating the H-aggregate behavior due to the dominated interchain coupling. It is noticed that with the increased content of 12-thiol, the PL intensity increased slightly, which may be owning to the introduction of 12-thiol changed the intrachain or interchain interactions among the P3HT polymer chains. Another plausible explanation could be that the addition of 12-thiol into P3HT solution had diluted the P3HT solution, which increased the PL intensity.

In order to elucidate the effect of the length of alkylthiols on the morphological transformation, besides 12-thiol, two other alkylthiols 7-thiol and 18-thiol were also chosen as additives. It showed that the influence posed by these two different alkylthiols was similar, that is, both of them could promote P3HT nanofibers transform into nanoribbon morphology with the flat-on orientation (**Figure 4**). The values of d_{020} and d_{100} calculated from SAED patterns of P3HT nanoribbons with the addition of different alkylthiols were listed in **Table 1**. Their d_{020} and

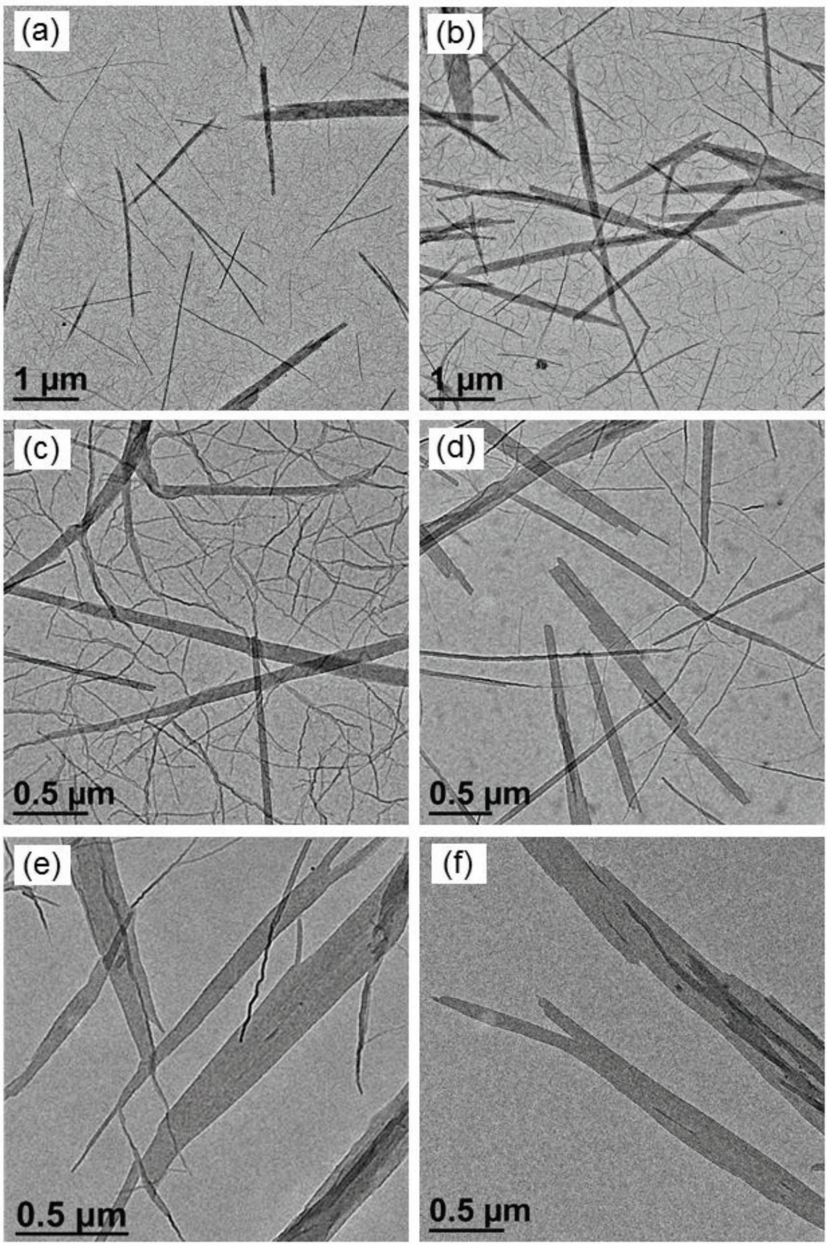

Figure 2. TEM images showing the morphological transformation from initial P3HT nanofibers to nanoribbons with the addition of different content of 12-thiol. a) 1%, b) 5%, c) 10%, d) 20%, e) 30%, and f) 50% by volume.

d_{100} were slightly different; however, the relationship between the length of alkylthiols and the lamellar spacing was not clear at present. We noticed the aggregation of nanoribbons with the addition of 18-thiol (Figure 4b). Since 18-thiol is a solid, the precipitated 18-thiol during the solvent evaporation process may cause the aggregation of P3HT nanoribbons with each other.

A possible mechanism was proposed to explain how the P3HT 1D nanofibers transformed into 2D nanoribbons during the addition of alkylthiols. Since there was no chemical reaction site between P3HT chains and alkylthiols, these alkylthiols mainly contributed to the morphology transition via physical interaction. Take 12-thiol as an example, the relative affinity of 12-thiol to P3HT was governed by the polymer–solvent interaction parameter,[29,30] χ_{P-S} (P = polymer and S = solvent), which can be estimated by $\chi_{P-S} = V_S\,(\delta_S - \delta_P)^2/RT + 0.34$, where V_S is the molar volume of the solvent, R is the gas constant, T is the Kelvin temperature, and δ_S and δ_P are the solubility parameters of the solvent and polymer, respectively. In the present work, the solubility parameters of P3HT and 12-thiol are 19.4 (J cm^{-3})$^{1/2}$ and 17.5 (J cm^{-3})$^{1/2}$,[13,30] respectively. By calculation, $\chi_{P3HT-12\text{-}thiol} = 0.69$. Using the Flory–Huggins criterion, the complete solvent–polymer miscibility can be realized when $\chi_{P-S} < 0.5$. Therefore, 12-thiol is a relatively poor solvent for P3HT. As we know, both π–π interactions between polymer backbones and van der Waals interactions between hexyl side chains play crucial roles in determining the crystallization and final morphology of P3HT. During the addition of 12-thiol, it played two roles at different stages: first as the additive to intercalate into the P3HT molecules, then as a poor solvent with the increased content. Initially, P3HT chains exhibit planarized conformation in $CH_2Cl_2/CHCl_3$ mixed solution and π–π stack with each other to form the nanofibers along (020) direction (**Figure 5**a). After the addition of 12-thiol, although it is a poor solvent for P3HT according to the calculated $\chi_{P3HT-12\text{-}thiol}$, it is a good solvent for the hexyl side chains of P3HT based on the principle of "like dissolves like." Even for 18-thiol as a solid, after it is dissolved in $CH_2Cl_2/CHCl_3$ mixed solution, it has good affinity to the hexyl side chains. Therefore, these alkylthiol molecules can intercalate into the gap of the adjacent hexyl side chains, interact with them and prevent them from interdigitation. As a result, van der Waals interactions between hexyl chains are strengthened. The strengthened hexyl interaction via the presence of alkylthiols promotes the remaining free P3HT chains in the solution to crystallize and grow along (100) direction, together with the alkylthiols intercalating into the gap between hexyl side chains, leading to the formation of nanoribbons (Figure 5b). Further increasing the amount of alkylthiols (e.g., with 50% of 12-thiol by volume), the solvent mixture became poorer to the P3HT chains, which strengthened the π–π stacking of P3HT with the increased shoulder peak observed in the UV–vis spectrum (Figure 3a).

We note that the key to the success in forming P3HT nanoribbons from as-prepared nanofibers is the use of additive with suitable structure (i.e., molecules with alkyl chains can strengthen the van der Waals force to promote side chain packing of P3HT), relative affinity and proper solubility for

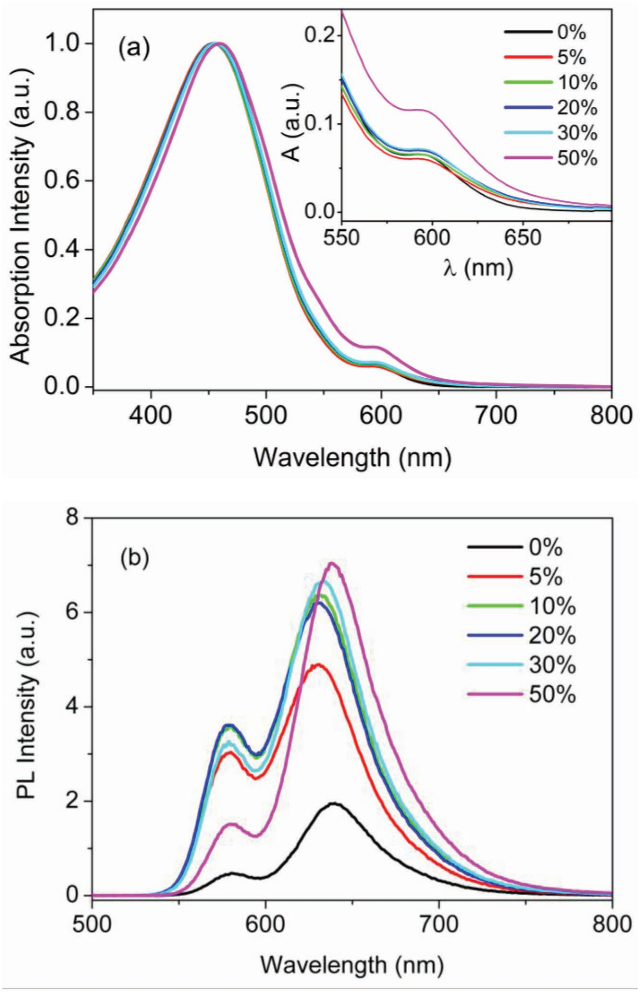

Figure 3. a) UV–vis and b) PL spectra of P3HT solution with the addition of different content of 12-thiol. The inset in (a) shows the detailed UV–vis spectra in the range of 550–700 nm.

Table 1. Summary of the d_{100} and d_{020} values of P3HT nanoribbons drop-cast from $CH_2Cl_2/CHCl_3$ solution with the addition of different alkylthiols at 30% by volume.

Additive	7-thiol	12-thiol	18-thiol
d_{100}/ Å	17.51	16.74	16.99
d_{020}/ Å	4.13	3.84	4.02

P3HT chains. For comparison, four different additives with different end groups (*n*-dodecane, dodecanoic acid, dodecyl amine, and oleylamine) were also employed and added into the P3HT nanofiber solution. These additives are poorer solvents for P3HT compared to the DDT based on the polymer–solvent interaction parameter, χ_{P-S} (Table S1, Supporting Information). Only aggregation of P3HT nanofibers or precipitations were observed with the addition of these additives, consistent with their pronounced vibronic shoulder peaks at longer wavelengths (550–620 nm) in UV–vis spectrum (Figure S4, Supporting Information).[31] This may be due to further crystallization of rod-like P3HT chains into fibrillar aggregates with π–π interaction as the dominant driving force. No obvious nanofiber-to-nanoribbon morphology transition was observed with the addition of these four additives, indicating these additives primarily promote π–π stacking instead of van der Waals force among P3HT chains.[32] In addition to the studies noted above, control experiment also showed that the concentration of P3HT was irrelevant to the nanofiber-to-nanoribbon morphology transition. When diluting the P3HT nanofiber solution from 0.5 mg mL^{-1} to 0.25 mg mL^{-1}, short and messy nanowhiskers were formed due to weaker interchain π–π stacking with decreased concentration (Figure S5, Supporting Information). When increasing the concentration of P3HT nanofiber solution to 5 mg mL^{-1}, more concentrated nanofibers were formed without the observation of nanofiber-to-nanoribbon transition (Figure S6, Supporting Information).

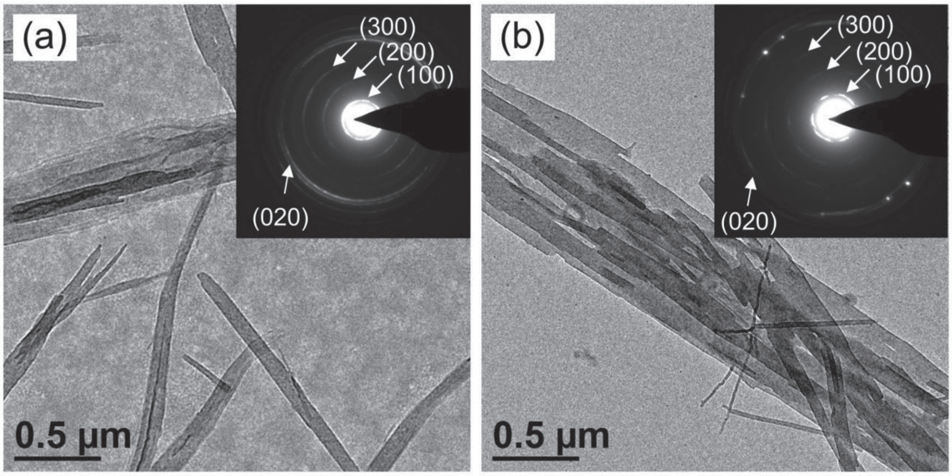

Figure 4. TEM images of P3HT nanoribbons drop-cast from $CH_2Cl_2/CHCl_3$ solution with the addition of a) 7-thiol and b) 18-thiol at 30% by volume. The insets are the corresponding SAED pattern.

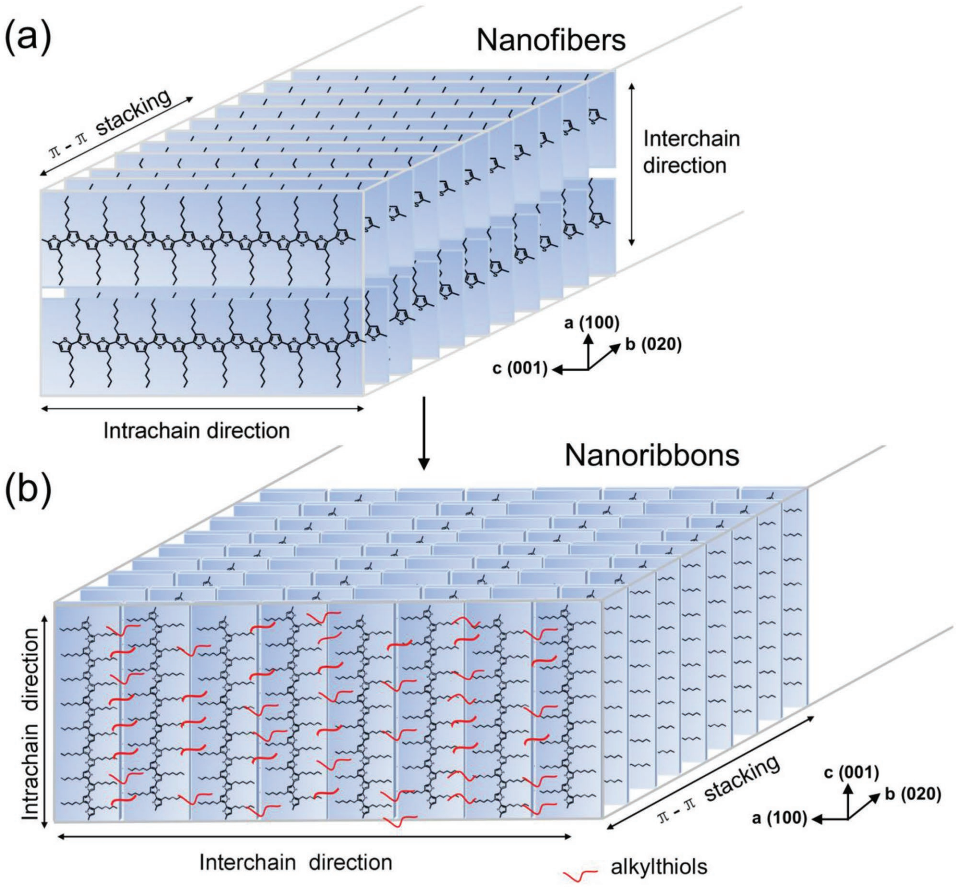

Figure 5. Schematic illustration of a) the P3HT molecular arrangement in nanofibers with an edge-on orientation and b) in nanoribbons after the addition of alkylthiol molecules (red lines) with a flat-on orientation, respectively.

4. Conclusion

In summary, we have demonstrated an interesting morphological transformation from P3HT 1D nanofibers to 2D nanoribbons via the addition of alkylthiols, accompanied by the crystallographic structures changing from edge-on orientation to flat-on orientation. Such transformation involves two-step crystallization of P3HT. Initially, P3HT chains assemble into nanofibers via π–π interactions. With the addition of alkylthiols, these small molecules intercalate into the free space of P3HT hexyl side chains and strengthen hexyl interactions via the favorable affinity between alkylthiols and hexyl side chains, which leads to the further growth of nanofibers along (100) direction to form nanoribbons. The correlation between P3HT morphological transformation and its photophysical properties is scrutinized. Overall, this work demonstrates an effective and simple way to control the P3HT crystal morphology and dimension. We expect that this strategy can be used into conjugated polymer-based OFETs, LEDs, solar cells, optical imaging, and sensors.

Supporting Information

Supporting Information is available from the Wiley Online Library or from the author.

Acknowledgements

This work was financially supported by the National Natural Science Foundation of China (Grant Nos. 21674024 and 21320102005) and Ministry of Science and Technology of China (2016YFA0203301). Z.L. acknowledges the Senior Visiting Scholarship of State Key Laboratory, Fudan University (17FGJ07).

Conflict of Interest

The authors declare no conflict of interest.

Keywords

conjugated polymers, crystal structures, nanoribbons, polythiophene, transitions

Received: January 17, 2018
Revised: March 13, 2018

[1] K. Zhang, Z. Hu, R. Xu, X. F. Jiang, H. L. Yip, F. Huang, Y. Cao, *Adv. Mater.* **2015**, *27*, 3607.
[2] Z. Fei, L. Chen, Y. Han, E. Gann, A. Chesman, C. R. McNeill, T. Anthopoulos, M. Heeney, A. Pietrangelo, *J. Am. Chem. Soc.* **2017**, *139*, 8094.

[3] Y. Wang, H. Cui, M. Zhu, F. Qiu, J. Peng, Z. Lin, *Macromolecules* **2017**, *50*, 9674.

[4] A. Marrocchi, D. Lanari, A. Facchetti, L. Vaccaro, *Energy Environ. Sci.* **2012**, *5*, 8457.

[5] M. Zhu, H. Kim, Y. J. Jang, S. Park, D. Y. Ryu, K. Kim, P. Tang, F. Qiu, D. H. Kim, J. Peng, *J. Mater. Chem. A* **2016**, *4*, 18432.

[6] X. Yang, J. Ge, M. He, Z. Ye, X. Liu, J. Peng, F. Qiu, *Macromolecules* **2015**, *49*, 287.

[7] B. Jung, K. Kim, Y. Eom, W. Kim, *ACS Appl. Mater. Interfaces* **2015**, *7*, 13342.

[8] G. Lu, L. Li, X. Yang, *Adv. Mater.* **2007**, *19*, 3594.

[9] M. He, L. Zhao, J. Wang, W. Han, Y. Yang, F. Qiu, Z. Lin, *ACS Nano* **2010**, *4*, 3241.

[10] J. Peet, C. Soci, R. Coffin, T. Nguyen, A. Mikhailovsky, D. Moses, G. C. Bazan, *Appl. Phys. Lett.* **2006**, *89*, 252105.

[11] L. Li, G. Lu, X. Yang, *J. Mater. Chem.* **2008**, *18*, 1984.

[12] J. Liu, S. Shao, H. Wang, K. Zhao, L. Xue, X. Gao, Z. Xie, Y. Han, *Org. Electron.* **2010**, *11*, 775.

[13] H. Wang, J. Liu, Y. Han, *Polymer* **2013**, *54*, 948.

[14] J. Peet, J. Y. Kim, N. E. Coates, W. L. Ma, D. Moses, A. J. Heeger, G. C. Bazan, *Nat. Mater.* **2007**, *6*, 497.

[15] J. K. Lee, W. L. Ma, C. J. Brabec, J. Yuen, J. S. Moon, J. Y. Kim, K. Lee, G. C. Bazan, A. J. Heeger, *J. Am. Chem. Soc.* **2008**, *130*, 3619.

[16] Y. Yao, J. Hou, Z. Xu, G. Li, Y. Yang, *Adv. Funct. Mater.* **2008**, *18*, 1783.

[17] W. Wang, H. Wu, C. Yang, C. Luo, Y. Zhang, J. Chen, Y. Cao, *Appl. Phys. Lett.* **2007**, *90*, 183512.

[18] X. Liu, S. Huettner, Z. Rong, M. Sommer, R. H. Friend, *Adv. Mater.* **2012**, *24*, 669.

[19] S. Pan, L. He, J. Peng, F. Qiu, Z. Lin, *Angew. Chem., Int. Ed.* **2016**, *128*, 8828.

[20] R. S. Loewe, P. C. Ewbank, J. Liu, L. Zhai, R. D. McCullough, *Macromolecules* **2001**, *34*, 4324.

[21] S. Samitsu, T. Shimomura, S. Heike, T. Hashizume, K. Ito, *Macromolecules* **2008**, *41*, 8000.

[22] E. B. Pentzer, F. A. Bokel, R. C. Hayward, T. Emrick, *Adv. Mater.* **2012**, *24*, 2254.

[23] Y. Han, Y. Guo, Y. Chang, Y. Geng, Z. Su, *Macromolecules* **2014**, *47*, 3708.

[24] J. Liu, M. Arif, J. Zou, S. I. Khondaker, L. Zhai, *Macromolecules* **2009**, *42*, 9390.

[25] R. J. Kline, D. M. DeLongchamp, D. A. Fischer, E. K. Lin, L. J. Richter, M. L. Chabinyc, M. F. Toney, M. Heeney, I. McCulloch, *Macromolecules* **2007**, *40*, 7960.

[26] L. Zhao, X. Pang, R. Adhikary, J. W. Petrich, M. Jeffries-EL, Z. Lin, *Adv. Mater.* **2011**, *23*, 2844.

[27] M. Baghgar, J. A. Labastide, F. Bokel, R. C. Hayward, M. D. Barnes, *J. Phys. Chem. C* **2014**, *118*, 2229.

[28] E. T. Niles, J. D. Roehling, H. Yamagata, A. J. Wise, F. C. Spano, A. J. Moulé, J. K. Grey, *J. Phys. Chem. Lett.* **2012**, *3*, 259.

[29] J. Brandrup, E. H. Immergut, E. A. Grulke, *Polymer Handbook*, 4th ed., John Wiley & Sons, New York **1999**.

[30] L. He, S. Pan, J. Peng, *J. Polym. Sci., Part B: Polym. Phys.* **2016**, *54*, 544.

[31] G. M. Newbloom, P. Iglesia, L. D. Pozzo, *Soft Matter* **2014**, *10*, 8945.

[32] W. Xu, L. Li, H. Tang, H. Li, X. Zhao, X. Yang, *J. Phys. Chem. B* **2011**, *115*, 6412.